Linear Parameter-Varying versus Linear Time-Invariant Control Design for a Pressurized Water Reactor

Pascale Bendotti [†]
Electricité de France
Direction des Etudes et Recherches
6 Quai Watier, 78401 Chatou, France

Bobby Bodenheimer [†]
College of Computing,
Georgia Institute of Technology,
801 Atlantic Drive, Atlanta, GA 30332-0280

September 15, 1998

Abstract

The applicability of employing a parameter-dependent control to a nuclear pressurized water reactor is investigated and is compared to that of using an $\mathcal{H}_\infty$ control. A linear time-invariant controller cannot maintain performance over the entire operating range. The parameter-dependent synthesis technique produces a controller which achieves specified performance against the worst-case time variation of a measurable parameter which enters the plant in a linear fractional manner. The plant can thus have widely varying dynamics over the operating range. The controllers designed perform well over the entire operating range.

Keywords: parameter-dependent control, gain-scheduling, $\mathcal{H}_\infty$ synthesis, system identification, nuclear reactor

1 Introduction

In France and certain other countries the major contribution to electricity production is provided by nuclear power. When this is the case, the nuclear power plant must provide electricity as it is needed and the plant becomes a time-varying system with dynamics changing slowly as the internal power changes. Nonetheless, large transients can occur, for example, when the plant shuts down. Most nuclear power plants are pressurized water reactors (PWR). The dynamics of a PWR change enough over its operating range that a linear time-invariant (LTI) controller cannot guarantee performance over the entire range, especially when operating conditions change suddenly.

[†]Completed while at California Institute of Technology, EE Dept., 116-81, Pasadena, CA91125

If a fixed LTI controller is not capable of maintaining performance over the entire operating range, then a possible approach to control a PWR is to design a parameter-dependent controller with the operating power as the parameter. One advantage such a controller would have over a standard gain-scheduled controller is that performance and stability could be guaranteed over the operating range of the plant, and large transients in switching are avoided. An additional advantage of linear parameter-varying (LPV) synthesis is that the controller is designed in one step, rather than by designing several controllers and then scheduling them. The potential drawback of LPV synthesis is that the technique is conservative. This conservatism may be so great that the controller performs quite poorly.

Previous work focused on related aspects of the control of a PWR. The dynamics change enough during the lifetime of the fuel that the controllers need to be periodically updated. This work investigated the applicability of employing μ-synthesis techniques to maintain the performance of a PWR over the entire lifetime of the fuel [1] [19].

In this paper our goal is control of this system over the operating range from 50% to 100% of its output power. We show the difficulties an LTI controller encounters because of the changing dynamics and how LPV control solves them. For the general control designer, the main points of interest are the construction of the parameter-varying model from identified, rather than analytic, models, and the use of a design weight which varies as the operating point changes. The material in this paper arose from previous work. In particular, the system identification and $\mathcal{H}_\infty$ control design were originally presented in [2, 3, 4] and the LPV synthesis in [5, 4]. The aim of this paper is to review the main results obtained and evaluate them using a realistic nonlinear simulator.

Section 2 reviews much of the theoretical machinery applied in this work. Section 3 is devoted to a description of the problem statement. Section 4 describes the identification and modelling of the plant. Section 5 presents the design of $\mathcal{H}_\infty$ controllers around two operating points. The main results of the chapter are presented in Sections 6 and 7 which describe the LPV synthesis and evaluation of the controllers.

2 Review of Linear Parameter-Varying Synthesis

We assume the reader has some familiarity with the fundamentals of feedback system analysis. In particular, we assume knowledge of the small-gain theorem and of memoryless operators. Willems [6] is an excellent reference for such material. The basic concepts of μ-analysis and μ-synthesis are also assumed; they can be found in Packard and Doyle [7]. Complete and rigorous explanations of this work can be found in [8, 7, 9].

The notation is standard. $\mathbb{R}$ and $\mathbb{C}$ denote the fields of real and complex numbers, respectively. $\mathbb{R}^k$ and $\mathbb{C}^k$ denote the real and complex k-dimensional vector spaces. $\mathbb{R}^{n\times m}$ and $\mathbb{C}^{n\times m}$ are the rings of real and complex $n \times m$ matrices. If $M \in \mathbb{C}^{n\times m}$, the maximum singular value of M is denoted by $\overline{\sigma}(M)$; $M^\star$ denotes the complex conjugate transpose. The Hilbert space of square summable

sequences is denoted by ℓ_2; $\mathcal{L}(\ell_2)$ represents the set of all linear time-varying operators on ℓ_2. The shift operator on ℓ_2 is denoted by $\mathbf{z}^{-1}$. For a rational transfer function matrix $G(\mathbf{z})$, if all poles of $G(\mathbf{z})$ are in the open unit disk, then $\|G\|_\infty = \max_{\omega \in [0,2\pi]} \overline{\sigma}\left[G(e^{j\omega})\right] = \max_{|\mathbf{z}|\geq 1} \overline{\sigma}\left[G(\mathbf{z})\right]$.

2.1 Linear Fractional Transformations

The background machinery for almost all results in this work is that of linear fractional transformations (LFTs). These were first introduced by Redheffer [10], but did not gain acceptance in the control community until the work of Safonov [11] and Doyle [12]. With LFTs, we can easily describe sets of systems as an operation between an operator and a matrix. All linear interconnections of systems and LFTs and more importantly, any rational function, can be represented as an LFT [13, 14].

Our notation for LFTs will be as follows. Let $\mathbf{\Delta}$ denote the set

$$\left\{\mathbf{diag}\left[\delta_0 I_{n_0}, \ldots, \delta_m I_{n_m}, \Delta_{m+1}, \ldots, \Delta_{m+F}\right] : \delta_i \in \mathcal{L}(\ell_2),\ \Delta_{m_j} \in \mathcal{L}(\ell_2)^{m_j \times k_j}\right\}.$$

Let $\mathcal{B}_{\mathbf{\Delta}} = \{\Delta \in \mathbf{\Delta} : \|\Delta\|_{\ell_2 \to \ell_2} \leq 1\}$. For each $\Delta \in \mathbf{\Delta}$, consider the loop equations

$$\begin{aligned} z &= P_{zv} v + P_{zu} u \\ y &= P_{yv} v + P_{yu} u \\ v &= \Delta z. \end{aligned}$$

This set of equations is shown pictorially as a block diagram in Figure 1, and we let

$$P = \begin{bmatrix} P_{zv} & P_{zu} \\ P_{yv} & P_{yu} \end{bmatrix}.$$

Usually P will be considered as a matrix of complex numbers. Its use in an LFT framework, however, gives it interpretations as a system and an operator depending on our set $\mathbf{\Delta}$. See [13, 14] for further details.

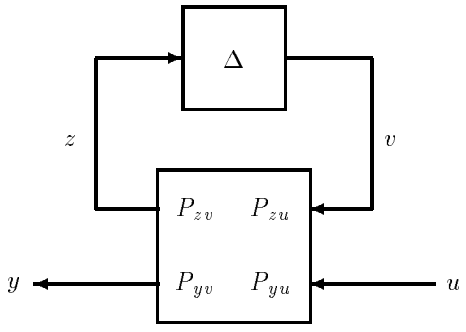

Figure 1: Block diagram representing a general LFT.

We can eliminate z and v from the loop equations, solving for y in terms of P, Δ, and u, which gives us

$$y = \left(P_{yu} + P_{yv} \Delta \left(I - P_{zv} \Delta \right)^{-1} P_{zu} \right) u \tag{1}$$

subject to the condition, which we shall henceforth assume, that $I - P_{zv}\Delta$ is invertible as an operator in $\mathcal{L}(\ell_2)$ for every $\Delta \in \boldsymbol{\mathcal{B}}_{\boldsymbol{\Delta}}$. The operator $\Delta \star P$ is said to be stable in this case. Equation 1 will be denoted as $y = (\Delta \star P)\, u$. Another common notation is $y = F_u(\Delta, P)u$.

In particular, when all $\delta_i \in \mathcal{L}(\ell_2)$ are time-varying (with a possible exception of one transform variable), then $\Delta \star P$ is stable for all $\Delta \in \boldsymbol{\mathcal{B}}_{\boldsymbol{\Delta}}$ if and only if there exists $0 < X \in \mathcal{T}$ and $0 < Y \in \mathcal{T}$ such that

$$P_{zv} X P_{zv}^{\star} - X < 0 \qquad P_{zv}^{\star} Y P_{zv} - Y < 0,$$

(see [15]) where $\mathcal{T}$ is referred to as the set of allowable transformations for $\boldsymbol{\Delta}$, and is as follows

$$\mathcal{T} = \left\{ T \in \mathbb{C}^{n \times n} : \det(T) \neq 0, T\Delta = \Delta T, \forall \Delta \in \boldsymbol{\Delta} \right\} \tag{2}$$

Furthermore, P is stabilizable with respect to $\boldsymbol{\Delta}$ iff there exists $X > 0$, $X \in \mathcal{T}$ such that

$$P_{zv} X P_{zv}^{\star} - X - P_{zu} P_{zu}^{\star} < 0.$$

If so, there exists a constant matrix F such that $A + BF$ is stable. Detectability follows by duality. A detailed discussion of these results can be found in [16]-[17].

2.2 $\mathcal{H}_\infty$ Synthesis

In this section we assume all systems are LTI. P will refer to the *generalized* plant, that is, what is normally called the plant, plus any weighting functions. Consider the standard feedback system shown in Figure 2. The vector signal w of exogenous inputs contains all disturbances, noises, and commands; e is the vector signal of quantities we wish to minimize; u and y are the controls and measurements, respectively.

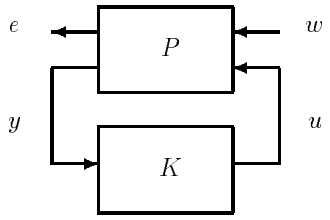

Figure 2: Feedback interconnection of P and K.

Roughly speaking, our goal is to find a controller K which minimizes the transfer function from w to e, denoted $P \star K$, in the sense of making the maximal energy captured by $P \star K$ small. This problem was elegantly solved by Doyle *et al.* in the classic paper [8].

The actual synthesis procedure is sub-optimal in the sense that a controller K is found such that $\|P \star K\|_\infty < \gamma$ for some pre-specified γ. There exists some optimal γ_o such that for all $\gamma < \gamma_o$ no stabilizing controller can be found for which the inequality holds. Optimal $\mathcal{H}_\infty$ controllers do not have many desirable qualities [18] and the standard practice is to approximate the optimal controller with a sub-optimal one for some desired tolerance. This procedure of minimizing the value of γ to a prescribed tolerance is known as *γ-iteration*. We may refer to a controller as being an $\mathcal{H}_\infty$ optimal controller: what we really mean is a sub-optimal controller to some tolerance.

Finally, note that in robust performance terminology, $\mathcal{H}_\infty$ synthesis is a one block technique, and this block is a performance block. When there is uncertainty present in the model, we will still perform $\mathcal{H}_\infty$ Synthesis by collecting all the uncertainty blocks into a diagonal structure with the performance block and covering this structure with one full block. This approach is conservative.

2.3 LPV Synthesis

In this section a brief overview of the LPV synthesis theory is presented. A complete and rigorous explanation of the synthesis technique can be found in [9].

Consider the general time-varying system shown in Figure 3, where $x(k), e(k), y(k), w(k)$, and $u(k)$ are the state, error, measurement, disturbance, and input vectors, respectively. We assume the time-variation of the plant can be represented as an LFT of a parameter set and a constant matrix. Thus $P(k)$ is given by

$$P(k) = \Delta(k) \star P \tag{3}$$

where

$$\Delta(k) = \mathbf{diag}\left[\delta_0(k) I_{n_0} \ldots \delta_m(k) I_{n_m}\right] \tag{4}$$

where each of the parameter variables δ_i is assumed to be a time-varying operator on ℓ_2 and satisfies $|\delta_i(k)| \leq 1$ for all $k \geq 0$ and $0 \leq i \leq m$, and n_i is the dimension of the identity matrix associated with δ_i. Notice that one δ_i may represent the shift operator. Equation 4 becomes $\Delta = [\mathbf{z}^{-1} I_{n_0}, \Delta]$. We assume that each δ_i can be measured on-line. Note that any system with rational time-varying entries can be represented in this framework, and many others can be arbitrarily closely approximated. This type of system is known as a parameter-dependent LFT system. The representation of P as an LFT is shown in Figure 4.

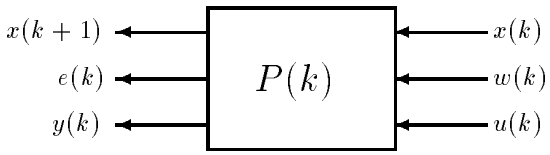

Figure 3: Time-varying system.

The controller we will design for this plant will also be parameter-dependent, depending on the same δ_i's as the plant; these copies are collectively denoted by $\widehat{\Delta}$. K thus has the form shown

in Figure 5. P can be augmented to collect all the time-varying parameters and states together; K can then be treated as a simple matrix. This is depicted in Figure 6, where R is the augmented form of P, and K is a matrix. The problem then appears as a robust control problem with a special structure on the plant and parameters. The design objective is to find a controller K such that the interconnection is stable and the $\ell_2 \to \ell_2$ induced norm from w to e is small for all allowable parameter variations $\Delta(k)$ (see Equation 4). Combining the gain from w to e with the gain of $R \star K$ (that is, treating the gain from w to e as a "performance block," another block in the $\mathbf{\Delta}$ structure) gives us a small-gain condition. Since the small-gain theorem can be quite conservative, we can reduce the conservatism by introducing scaling matrices from the set $\mathcal{T}$, given in Equation 2. Recall from Section 2.1 such matrices commute with the set of parameter variations.

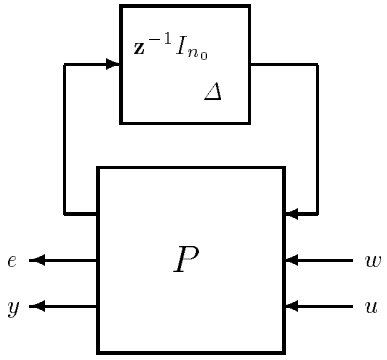

Figure 4: Parameter-dependent plant. The $\mathbf{z}^{-1}I_{n_0}$ term represents the states of P, and the Δ represents the time variation of Equation 4.

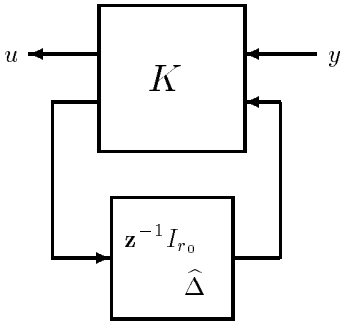

Figure 5: Parameter-dependent controller; $\mathbf{z}^{-1}I_{r_0}$ represents the states of the controller and $\widehat{\Delta}$ the time variations.

The resulting condition is then the state-space upper bound (SSUB) of [7]. This condition now becomes (compare Lemma 3.1 of [9] and Theorem 10.4 of [7]):

Theorem 1 *Let R be given as above, along with an uncertainty structure $\mathbf{\Delta}$. If there is a $T \in \mathcal{T}$*

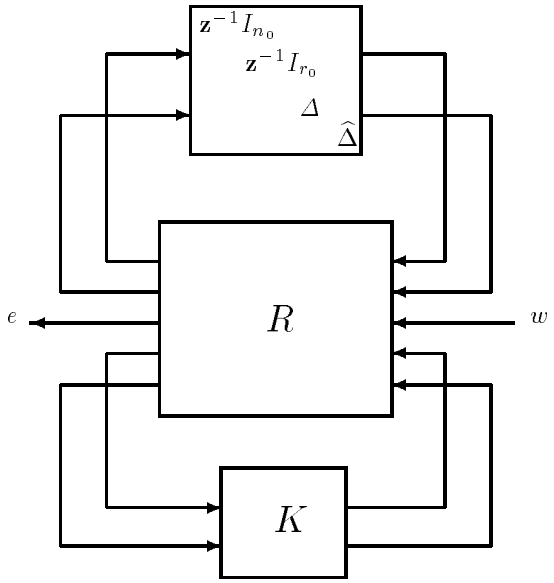

Figure 6: Parameter-dependent closed-loop system.

and a stabilizing, finite-dimensional, time-invariant K such that

$$\left\| \begin{bmatrix} T & 0 \\ 0 & I \end{bmatrix} (R \star K) \begin{bmatrix} T^{-1} & 0 \\ 0 & I \end{bmatrix} \right\|_\infty < 1 \tag{5}$$

then there is a γ, $0 \leq \gamma < 1$, such that for all parameter sequences $\delta_i(k)$ with $|\delta_i(k)| \leq 1$ for all $k \geq 0$, the system in Figure 6 is internally exponentially stable, and for zero initial conditions, if $w \in \ell_2$, then $\|e\|_2 \leq \gamma \|w\|_2$.

Pictorially, this theorem is shown in Figure 7. A natural question arising from this theorem is when does such a K exist for any value of γ, not just $\gamma < 1$? It is a simple corollary of results in [16] that such a K will exist when R is stabilizable and detectable with respect to the block structure (see definition given in Section 2.1) $\mathbf{\Delta} = \mathbf{diag}\left(\mathbf{z}^{-1}I_{n_0}, \mathbf{z}^{-1}I_{r_0}, \Delta, \widehat{\Delta}\right)$.

The important fact resulting from Theorem 1 is that the synthesis of T and K to meet the objective can be cast as a computationally tractable convex optimization problem involving 3 LMIs. These LMIs have the following form

$$U_\perp^T \left(E \begin{bmatrix} X & 0 \\ 0 & I \end{bmatrix} E^T - \begin{bmatrix} X & 0 \\ 0 & I \end{bmatrix} \right) U_\perp < 0,$$

$$V_\perp \left(E^T \begin{bmatrix} Y & 0 \\ 0 & I \end{bmatrix} E - \begin{bmatrix} Y & 0 \\ 0 & I \end{bmatrix} \right) V_\perp^T < 0,$$

$$\begin{bmatrix} X & I \\ I & Y \end{bmatrix} \geq 0,$$

where $U_\perp$, $V_\perp$, and E are obtained from the system realization, and X and Y are structured positive definite matrices. Interested readers may find the exact LMIs in Theorem 6.3 of Packard [9].

E, U, and V have a scaling γ absorbed into them, and thus the synthesis procedure is a γ-iteration, as $\mathcal{H}_\infty$ is. Once a desired γ level has been reached, a controller K can be obtained by linear algebraic operations on X and Y.

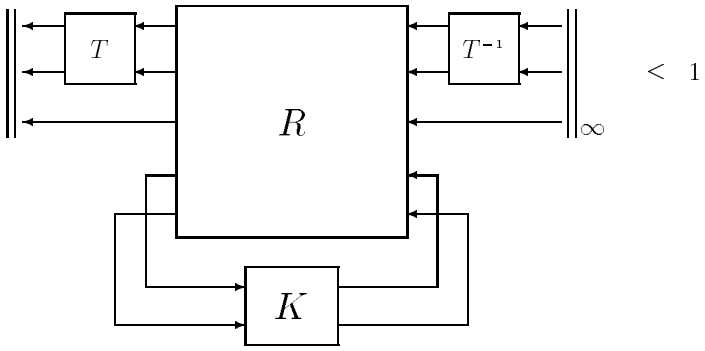

Figure 7: Diagram of Theorem 1.

A few points are important in understanding the ramifications of employing the state-space upper bound (SSUB). Most importantly, this technique results in a controller optimal with respect to a time-varying perturbation with memory (the sequence $\Delta(k)$ of Equation 4, becomes a time-varying operator with memory, rather than a sequence of complex numbers). The relationship between such an operator and a parameter useful in gain-scheduling is tenuous, at best. Depending on the problem, this technique could conceivably yield controllers so conservative as to have extremely poor performance. Nonetheless, if a controller with acceptable performance can be designed with this technique, then it will have at least the same level of performance for all variations of the operating point (the operating point is a fixed value of Δ). Additionally, a time-varying operator with memory does not in general have a frequency spectrum, so there is no way to "filter" it to achieve a closer relationship to an operating parameter. Moreover, it is interesting to contrast this technique with μ-synthesis where instead of the SSUB the frequency-domain upper bound is usually employed; this difference reflects the different assumptions about the type of perturbations.

If Δ is a constant value and is "wrapped into" the plant, the resulting model becomes a linear time-invariant model around the operating point of the Δ. Similarly, we can do this for controllers, and the LPV controller becomes a linear time-invariant controller. We will refer to the LTI controller obtained by holding Δ at a constant value as the LPV controller *locked* at the value of Δ. We are interested in looking at controllers locked in various positions because by comparing them with the full LPV controller we hope to gain better insight into the nature of LPV control.

3 Problem Statement

3.1 Description of the primary circuit

Consider the application depicted in Figure 8. This is the primary circuit of a PWR, and our goal is to control this part of the reactor.

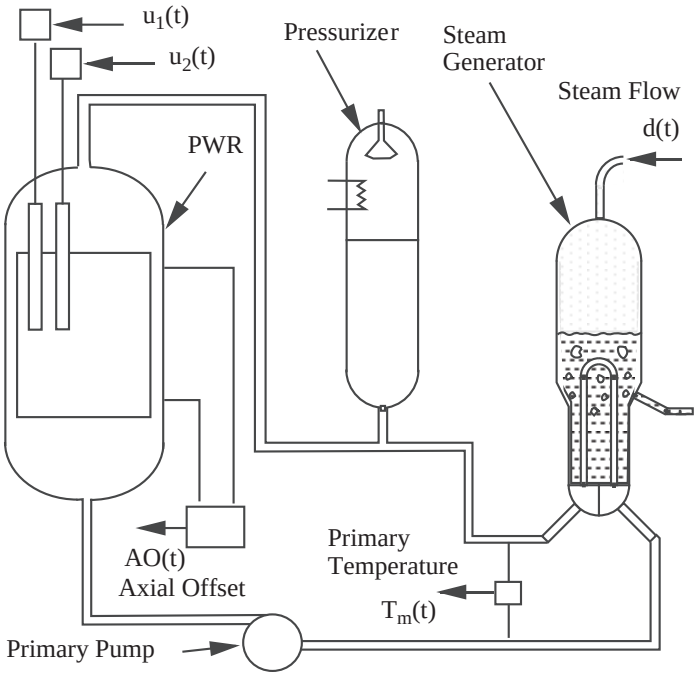

Figure 8: Primary circuit and steam generator.

The pressurized water in the primary circuit transmits the heat generated by the nuclear reaction to the steam generator. The rate of the reaction is regulated by the control rods. The rods capture neutrons, slowing down the nuclear reaction; withdrawing the rods increases the reaction.

Because of the way in which the control rods enter the reactor, the rate of reaction is always higher at the bottom of the reactor. The *axial offset* is defined as the difference in power generated between the top and bottom of the PWR. Safety specifications require minimizing the axial offset; this also increases the lifetime of the fuel and reduces operating costs.

The pressurizer has an inner control loop which holds the pressure in the primary circuit constant. In the steam generator, water of the secondary circuit turns into hot steam, which drives a turbo-alternator to generate electricity.

3.2 Control Objective

The main objective in controlling a PWR is to provide the commanded power while respecting certain physical constraints. Since the generated power in the secondary circuit, noted $\mathcal{P}$, is closely

related to the steam flow, we will assume in the sequel both signals equal. Hence, the required power corresponds to a specific steam flow that may be viewed as a measurable disturbance. The pressure is held constant, thus for a steam flow increase in the secondary circuit, the temperature in the primary circuit will decrease. From the primary circuit standpoint, one natural control objective is to track a temperature reference derived from the steam flow. A secondary objective is to minimize the axial offset to comply with safety specifications.

To achieve such objectives, two sets of rods are available as control. The rates of motion of the control rods are denoted u_1 and u_2, respectively; the positions of the rods are denoted v_1 and v_2, respectively. The positions are measurable. Due to the physics of the reactor, u_2 has more authority than u_1 at low power and using it results in a smaller axial offset. At high power, however, u_2 has almost no authority, so all control must come from u_1. Furthermore, the dynamics of a PWR change with both the operating power and the reactivity of the fuel during the lifetime of the reactor [19].

Due to the complexity of the physical plant, performance specifications cannot be uniquely or easily derived. Moreover, safety specifications require basically that any meaningful physical variable lies in a pre-specified domain. Thus, it makes the control problem mainly driven by constraints. In the unconstrained setting, the problem is to derive performance specifications that are consistent with the actual constraints. The idea is to have, as much as possible, the same closed loop behavior with and without constraints. Indeed, investigations into the best performance specifications are currently underway at Electricité de France (EDF). Below are the first attempts to automatically control the axial offset, a specification we will also use here. Nonetheless, we do not have precise specifications the controllers must meet.

4 System Identification and Modelling

The first step of any design procedure is to obtain a model. Here we review the identification process for the PWR. Our goal is to obtain a reasonably low order model for the plant.

4.1 Identification Experiments

The identification experiments were carried out using a realistic nonlinear simulator developed at EDF. The simulator is based on various finite element models of the PWR.

The system possesses nonlinearities of two types. The first depends on the operating condition and hence is strongly related to the commanded power. No *a priori* knowledge can be used in the identification process for this type of nonlinearity, so the nonlinear (NL) simulation data are obtained around different operating points and the resulting model is a linearization at the operating point. The second nonlinearity is on the input magnitude of v_2. This control becomes ineffective when the commanded power tends to its maximum. This maximal value is usually referred to as

the nominal power of the plant, $\mathcal{P}_n$. The static characteristic of the input effectiveness is actually known, so its inversion allows identification close to the nominal power, where the nonlinear effect is maximal.

4.2 MIMO State-space Description

Consider the system depicted in Figure 9, where T_m, AO, P_I, d, v_1 and v_2 are the temperature, the axial offset, the primary power, the steam flow and the vertical positions of the rods, respectively. Recall from Section 3 that, from the primary circuit control standpoint, the steam flow is a disturbance, thus it needs to be an input in the identification process.

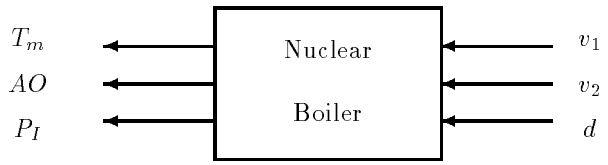

Figure 9: Input/Output diagram of the primary circuit.

The physical system is described by an LTI system around an operating point given by the following:

$$\begin{bmatrix} x(k+1) \\ y_s(k) \end{bmatrix} = \begin{bmatrix} A & B \\ C & D \end{bmatrix}, \begin{bmatrix} x(k) \\ v(k) \\ d(k) \end{bmatrix} \tag{6}$$

with

$$y_s(k) = \begin{bmatrix} T_m(k) \\ AO(k) \\ P_I(k) \end{bmatrix} \quad \text{and} \quad v(k) = \begin{bmatrix} v_1(k) \\ v_2(k) \end{bmatrix}$$

where $x(k)$, $y_s(k)$, $v(k)$, and $d(k)$ represent the state, the output, the input, and the disturbance at time k, respectively. The parameters of the state-space realization consist of the elements of the A, B, C, D, and , matrices.

Since the number of parameters rises quadratically with the state dimension, there are a large number of them in a state-space realization. To meaningfully reduce them, specific realizations are used where some parameters are fixed at either zero or one, for example, the well known MIMO canonical forms. Unfortunately, these realizations still contain too many parameters to be uniquely identified.

Re-parameterizing the realizations using physical considerations can overcome this problem. Preliminary identification of several SISO and MISO transfer functions are performed providing insight into an appropriate re-parameterization (*cf.* references in [2]). Indeed, the primary temperature and power are mainly related to the control inputs by a second and first order system,

respectively. Furthermore, the inputs affect the plant dynamics in an identical manner, although the gains are different. The axial offset is almost a linear combination of the inputs: thus no states are needed for it. These insights provide an appropriate identification-oriented state-space realization structure. Hence, only the temperature and the power have dynamics. The effect of the disturbance has a larger delay than the effect of the control and hence the dimension of the state must reflect this. More precisely, 3 delay values for each of temperature and power (instead of 2 and 1, respectively, in the disturbance-free case) are required to appropriately predict the input-output behavior. This leads to a sixth order state-space realization defined as follows:

$$\left[\begin{array}{c|cc} A & B & , \\ \hline C & D & 0 \end{array}\right] = \left[\begin{array}{cccccc|ccc} 0 & 1 & 0 & 0 & 0 & 0 & b_1^1 & b_2^1 & 0 \\ 0 & 0 & 1 & 0 & 0 & 0 & 0 & 0 & 0 \\ a_1^{11} & a_2^{11} & a_3^{11} & 0 & a_2^{12} & 0 & 0 & 0 & \gamma_3 \\ 0 & 0 & 0 & 0 & 1 & 0 & 0 & 0 & 0 \\ 0 & 0 & 0 & 0 & 0 & 1 & 0 & 0 & 0 \\ a_1^{21} & 0 & 0 & a_1^{22} & a_2^{22} & a_3^{22} & 0 & 0 & \gamma_6 \\ \hline 1 & 0 & 0 & 0 & 0 & 0 & 0 & 0 & 0 \\ 0 & c_2^2 & 0 & c_4^2 & 0 & 0 & d_2^1 & d_2^2 & 0 \\ 0 & 0 & 0 & 1 & 0 & 0 & d_3^1 & d_3^2 & 0 \end{array}\right]. \quad (7)$$

The state matrix A can be partitioned as follows:

$$A = \left[\begin{array}{cc} A_{11} & A_{12} \\ A_{21} & A_{22} \end{array}\right]$$

where A_{11} and A_{22} denote the third order systems for the temperature and the power; A_{12} and A_{21} represent the cross-coupling matrices which contain only one non-zero term, appropriately located. The input matrix B accounts for the actual delayed effect of the control inputs on primary temperature and power, so only the first row of B has non-zero elements. Similarly, the delay between the control inputs and the disturbance can be taken into account using only the third and sixth elements of the disturbance input matrix , . The second row of the output matrix C adds memory to the axial offset. Finally, the elements of D correspond to the direct terms appearing in the axial offset and the power. This results in a specific identification-oriented realization with 18 parameters, instead of the 28 parameters in the standard canonical form.

4.3 MIMO Identification

Similarly, the overall system (6) can also be modelled by the transfer function:

$$y_s(k) = G_v(\theta, q)v(k) + G_d(\theta, q)d(k) \quad (8)$$

where q denotes the standard forward shift operator (the corresponding **z** operator will be omitted for simplicity), and θ represents the vector of free parameters to be identified.

Given a description (8) properly parameterized by the specific form (7) and the input–output data v, y_s and d, the prediction error ε is computed as follows:

$$\varepsilon(k) = y_s(k) - G_v(\theta, q)v(k) - G_d(\theta, q)d(k).$$

The identification method consists in determining the parameter estimates by minimizing the following quadratic criterion:

$$\widehat{\theta} = \arg\min_{\theta} \det \left[\frac{1}{N} \sum_{k=1}^{N} \varepsilon(k)\varepsilon^T(k) \right]$$

using an iterative Gauss-Newton algorithm [20].

4.4 Confirmation and Results

Finally, we confirm the identified model is accurate by checking how well it predicts the behavior of the physical system when simulated with a different data set to see how well it matches the actual output of the physical system. This procedure was successful over a large operating range due to the static inversion performed at the plant input. In particular, the specific form used for the parameterization was verified.

The time-domain responses of the identified model obtained around $0.5\mathcal{P}_n$ (dashed) are plotted against the NL simulation data (solid) in Figure 10. The inputs used to generate this data — v_1 (solid), v_2 (dashed) and d (dotted) — are plotted in the right lower diagram in Figure 10. The step-responses of the identified models obtained around $0.5\mathcal{P}_n$, $0.9\mathcal{P}_n$ and $0.99\mathcal{P}_n$, called $\widehat{G}_0$, $\widehat{G}_1$, and $\widehat{G}_2$, respectively, are shown in Figure 11.

4.5 Model Reduction

Since our design methods yield controllers with state dimension equal to that of the open-loop interconnection structure, often we can reduce the order of the controller by reducing the plant model before controller synthesis. In the present case we are reducing the sixth order models. A balanced realization technique [21], including specified model reduction weightings, is used [22].

In particular, dynamic behavior at high frequencies can be considered uncertainty. Therefore, the measurements are weighted with low-pass filters to attenuate the high frequency dynamics. Finally, the reduced order model is obtained by truncating weakly controllable and observable states. The resulting MIMO reduced order plant model is first order, i.e., only the dominant mode is retained.

The nominal reduced order plant model is the design model G_0 while the nominal plant model is $\widehat{G}_0$. Figure 11 shows the step-responses of $\widehat{G}_0$ in solid lines against those corresponding to G_0 in dashed lines. For purposes of comparison, those corresponding to $\widehat{G}_1$ (dotted) and $\widehat{G}_2$ (mixed) are plotted on the same graphs.

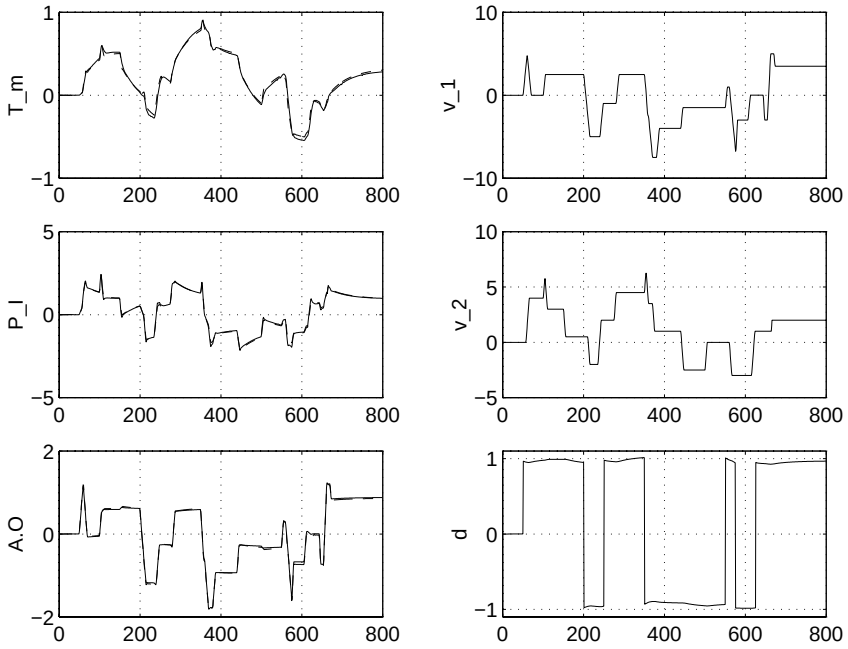

Figure 10: NL Simulation data versus time-domain responses of $\widehat{G}_0$. The data is in solid lines, and the time response in dashed lines.

Due to the lower order approximation, model inaccuracy is unavoidable. Since the high frequency dynamics are no longer modelled, there is a significant difference between the identified model and the reduced order model. Figure 12 shows the Bode plots corresponding to the multiplicative-errors relating the design model G_0 to $\widehat{G}_0$ (dashed), $\widehat{G}_1$ (mixed) and $\widehat{G}_2$ (dotted), respectively. '$\widehat{\ }$' is replaced by '$\widetilde{\ }$' to denote these errors. Please note, the figure also contains the uncertainty weight which will be explained later.

4.6 Parameter Dependence

Our model in the form of Equation 3 will be derived using the first-order models of the previous section with the operating power $\mathcal{P}$ as the parameter. To derive the parameter dependence, each term of the three first-order models is compared; those which vary are individually fitted with a rational function of δ_1, using a least-squares technique. For the PWR, first order LFTs of the form $e + f\delta_1(1-g\delta_1)^{-1}h$ fit the parameters extremely well, as shown in Figure 13. The parameter variation is normalized using $\mathcal{P} = (\delta_1 + 3)/4$ such that $-1 \leq \delta_1 \leq 1$. Thus, $0.5\mathcal{P}_n$ corresponds to $\delta_1 = -1$, $0.9\mathcal{P}_n$ corresponds to $\delta_1 = 0.6$, and $0.99\mathcal{P}_n$ to $\delta_1 = 0.998$ (these are the asterisks in the figure). The resulting model with δ_1-dependence, G_{δ_1}, becomes

$$\left[\begin{array}{c|c} A & B \\ \hline C & D \end{array}\right] = \left[\begin{array}{c|ccc} a(\delta_1) & b_{v_1}(\delta_1) & b_{v_2}(\delta_1) & b_3 \\ \hline c_1 & d_{11} & d_{Tm_2}(\delta_1) & d_{13} \\ c_2 & d_{21} & \kappa b_{v_2}(\delta_1) & d_{23} \\ c_{AO}(\delta_1) & d_{AO_1}(\delta_1) & d_{32} & 0 \end{array}\right]. \tag{9}$$

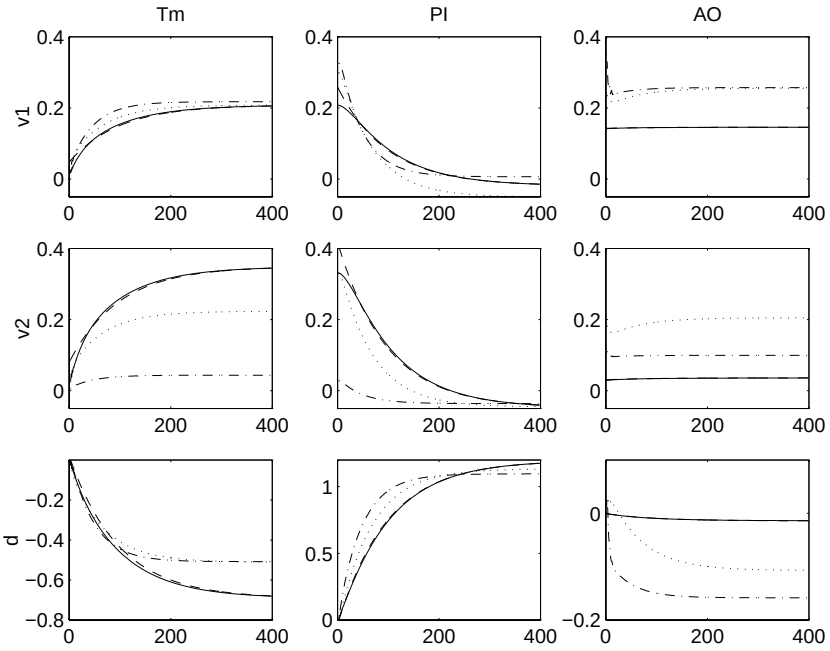

Figure 11: Step-responses of $\widehat{G}_0$ (solid), G_0 (dashed), $\widehat{G}_1$ (dotted) and $\widehat{G}_2$ (mixed).

The inputs for this model are the vertical positions v_1, v_2, and the steam disturbance d; the outputs are the mean temperature T_m, the primary power P_I, and the axial offset AO, respectively (see Figure 8). Placing this model in the form of Equation 3 results in a system shown in Figure 4, where $n_0 = 1$ and $n_1 = 6$, that is $\Delta = \mathbf{diag}[\mathbf{z}^{-1}, \quad \delta_1 I_6]$.

From Figure 13, notice the system matrix $a(\delta_1)$ is inversely proportional to the operating power and the time constant changes by a factor of 2 over the operating range. Also, the variation of b_{v_2} and d_{P_2} differs only by a constant, κ, which is used to reduce the size of the final Δ-block. More importantly, the effectiveness of u_2 decreases as the power increases, and is almost zero at full power. The gain in the axial offset channel increases as power increases, making it more difficult to control at high power. In particular, the effect of u_1 on the axial offset (d_{AO_1}) increases, while the effect of u_2 decreases. This makes it practically impossible to require any performance on axial offset at high power.

5 $\mathcal{H}_\infty$ Controller Design

The first controllers are designed using an $\mathcal{H}_\infty$ methodology; this gives us a first approximation for the weights used in LPV synthesis. Recall that $\mathcal{H}_\infty$ synthesis is aimed at disturbance rejection. A tracking problem such as the PWR can be cast as disturbance rejection by rejecting the low frequency components of the error between plant output and the reference. As the synthesis is in continuous-time, the weighting functions are specified in continuous-time as well. Then the discrete-time $\mathcal{H}_\infty$ controller is obtained using the bilinear transformation. The LPV design is

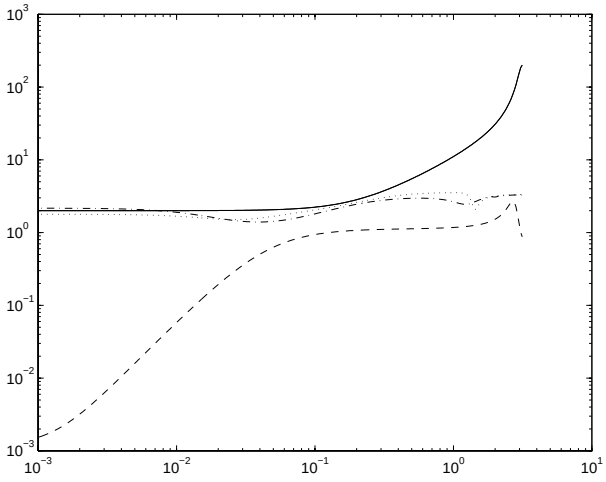

Figure 12: Uncertainty weight and relative errors relating G_0 to $\widehat{G}_0$, $\widehat{G}_1$, $\widehat{G}_2$, respectively. The error $\widetilde{G}_0$ is in dashed lines, $\widetilde{G}_1$ is in mixed lines, $\widetilde{G}_2$ is in dotted lines and w_m is in solid lines

carried out in discrete-time.

5.1 Uncertainty Description

As the controllers must stabilize the actual plant, our design methodology must account for the discrepancy between model and reality. We employ the standard approach of designing a controller stabilizing the nominal model in the presence of modelling errors.

A multiplicative-error is used to provide a description of the plant mismatch as well as a characterization of robust stability.

Consider the design model G_0 and rewrite it as follows:

$$\begin{bmatrix} y_1(k) \\ y_2(k) \end{bmatrix} = \underbrace{\begin{bmatrix} G_{v1} & G_{d1} \\ G_{v2} & G_{d2} \end{bmatrix}}_{G_0} \begin{bmatrix} v(k) \\ d(k) \end{bmatrix} \tag{10}$$

where y_1 denotes the controlled outputs and y_2 is an auxiliary output:

$$y_1(k) = \begin{bmatrix} T_m(k) \\ AO(k) \end{bmatrix} \text{ and } y_2(k) = P_I(k).$$

The plant model description corresponding to the identified plant model $\widehat{G}_0$ in (8) is obtained by replacing G with $\widehat{G}$ in (10).

Given a nominal model G_{v1} as well as the weighting function W_m, the multiplicative model set is defined as:

$$\Sigma(G_{v1}, W_m) = \{G_{v1}(I + \Delta_2 W_m) \mid \Delta_2 \text{ stable}, \|\Delta_2\|_\infty \leq 1\}.$$

A typical robust stability test for multiplicative perturbations is to find a stabilizing controller

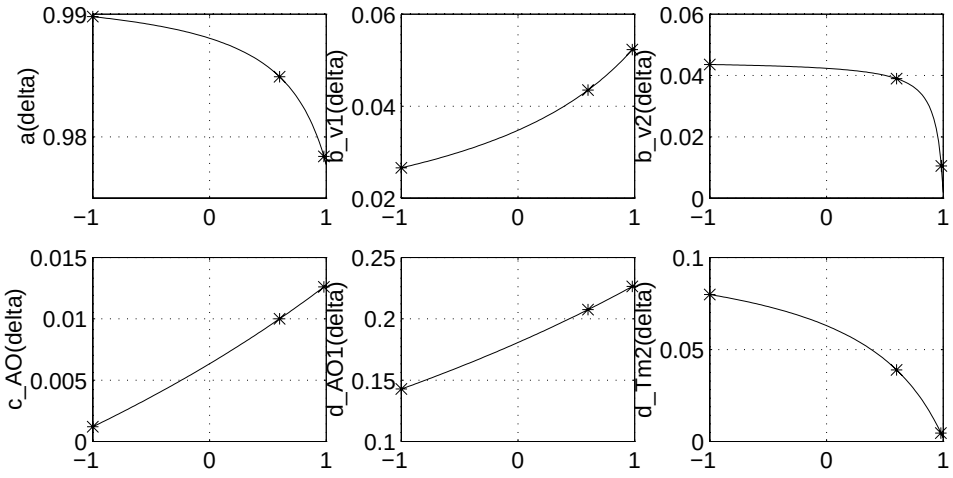

Figure 13: Parameter variations versus δ_1 for the model of Equation 9. A '*' shows an actual value, and the line shows the LFT fit.

K which satisfies

$$\forall\omega \quad \bar{\sigma}(W_m T) \leq 1 \iff \|W_m\, T\|_\infty \leq 1 \implies \|T\|_\infty \leq \|W_m\|_\infty^{-1} \tag{11}$$

where $T = KG(I + KG)^{-1}$ is the plant input complementary sensitivity function and W_m is the multiplicative uncertainty weight specifying the amount of uncertainty in the model as a function of frequency.

In the present case, the uncertainty weight is of the form $W_m = w_m I_2$, where w_m is a stable minimum-phase scalar valued function and has a large magnitude in the frequency range where the modelling error is too large; w_m is chosen as follows:

- In the frequency range where known dynamics have been neglected,

$$|w_m| \geq \|G_{v1}^{-1}(\widehat{G}_{v1} - G_{v1})\|_2 \tag{12}$$

  where $\widehat{G}_{v1}$ is the identified transfer function from v to y_1 while G_{v1} is the corresponding transfer of the nominal reduced order model (as shown in Equation 10).

- Outside the frequency range of the experiment, $|w_m|$ is large to account for unmodelled dynamics.

Figure 12 shows $w_m(\mathbf{s}) = \frac{200\mathbf{s}+20}{\mathbf{s}+10}$ (solid) and the relative modelling errors (12) relating G_0 to $\widehat{G}_0$ (dashed), $\widehat{G}_1$ (mixed) and $\widehat{G}_2$ (dotted), respectively[1].

5.2 Performance Specifications

The synthesis structure is shown in Figure 14. The design model includes the actuator dynamics, modelled by two integrators and denoted by *Act*. Also, the vertical positions of the control rods

[1] The weight is given in continuous-time using the Laplace transform s.

and the disturbance d are measured. In this figure, d, n, r, u, and y refer to the disturbance, noise, reference, control, and measurement signals, respectively. This synthesis structure leads to a one degree of freedom (1DOF) controller, thus the controller inputs are the tracking errors or the measured outputs. In the latter case, no reference is specified and the signal r represents noise. Note that this structure involves a feedforward on the disturbance since this signal is measured.

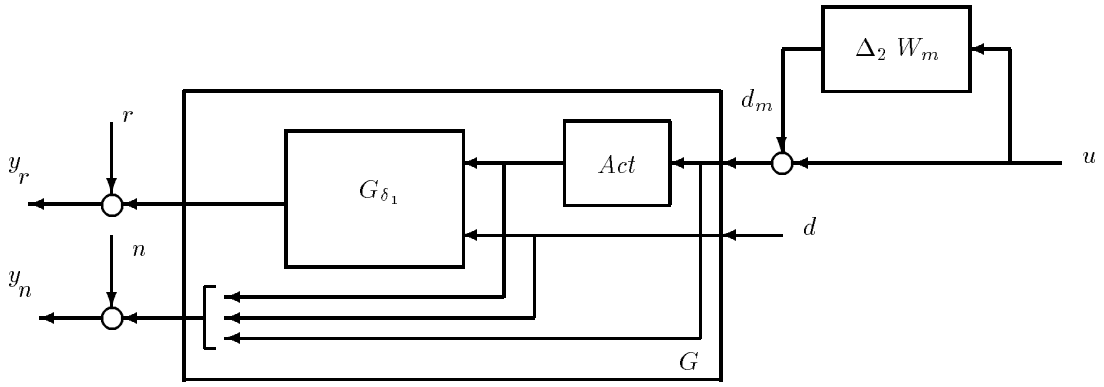

Figure 14: Synthesis structure for the PWR.

To have nominal performance we attempt to find a controller K which satisfies

$$\forall\omega \quad \bar{\sigma}(W_p S) \leq 1 \quad \Longleftrightarrow \quad \|W_p\ S\|_\infty \leq 1 \quad \Longrightarrow \quad \|S\|_\infty \leq \|W_p\|_\infty^{-1} \tag{13}$$

where $S = (I + GK)^{-1}$ denotes the plant output sensitivity function and W_p denotes the diagonal weighting matrix reflecting the performance specifications. W_p is given as follows:

$$\begin{aligned} W_p &= \mathbf{diag}[W_{T_m}, W_{P_I}, W_{AO}, W_{pos}] \\ &= \mathbf{diag}\left[\frac{0.01(\mathbf{s}^2 + 1.2522\mathbf{s} + 0.8)}{\mathbf{s}^2 + 0.0056\mathbf{s} + 1.610^{-6}}, 5, 2, 0.45I_2\right]^1 \end{aligned}$$

which weights the performance on temperature, power, axial offset, and vertical position of the control rods. To insure low steady-state error in tracking and to reject step disturbances, W_{T_m} resembles an integrator. As a second objective, the control strategy should minimize the effect of the control on the axial offset. A constant weight W_{AO} is introduced on the axial offset (dotted lines). This causes the use of u_2 to be preferred over u_1 since it has more authority at low power and results in lower axial offset. Because the system has fewer degrees of freedom than performance measures, it is only possible to minimize the axial offset, not to reject it.

To limit the magnitude of the positions of the control rods, a constant weight W_{pos} is used (dotted lines). As an aside, it is interesting to note that if W_{pos} is omitted, both the $\mathcal{H}_\infty$ and LPV methods will produce controllers which give a dramatically lower axial offset. They do this by moving the control rods in opposition to one another, which clearly will produce lower power generation at the top and bottom of the vessel. Unfortunately, this type of motion is not physically possible on this reactor. We eliminate it by placing a penalty on the movement, which works since

when the rods move in opposition to one another, they must move more to achieve the same affect on the temperature. Penalizing their movement causes them to move together, at the expense of the axial offset.

The synthesis structure shown Figure 14 can be redrawn in a more standard way as depicted in Figure 15.

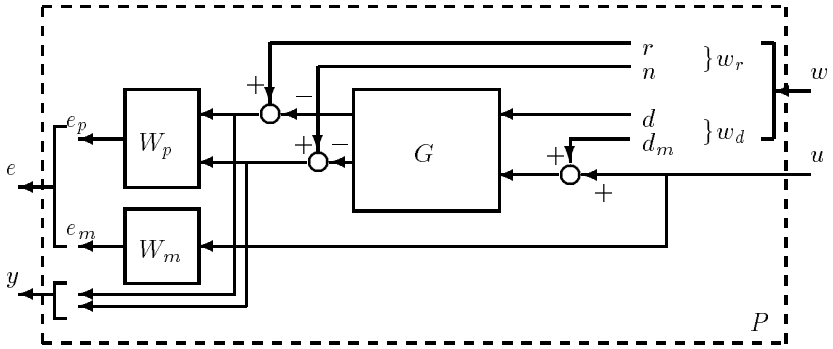

Figure 15: Augmented plant P for the PWR.

Consider the two sets of inputs

$$w_r = \begin{bmatrix} r \\ n \end{bmatrix}, \; w_d = \begin{bmatrix} d \\ d_m \end{bmatrix}$$

where w_r defines the reference and measurement noise at the plant output, and w_d represents the disturbance at the plant input. The structure has also two sets of outputs, noted e_p and e_m. The generalized plant P consists of 4 blocks arranged 2×2 and the corresponding Δ structure presents two blocks on the diagonal. The robust performance objective is achieved if

$$\|P \star K\|_\infty = \left\| \begin{array}{cc} W_p S & W_p SG \\ W_m KS & W_m KSG \end{array} \right\|_\infty \leq 1 \tag{14}$$

Note that for multivariable systems, $KSG = KG(I + KG)^{-1} = T$.

Recall from Section 2.2 that our two block problem is treated as an $\mathcal{H}_\infty$ problem by covering the uncertainty structure with one full block and not exploiting the structure of the problem. This is conservative, and the diagram is drawn as an implicit two block problem to remind us of that.

5.3 Synthesis

Once the weights have been selected, the design process is simply an iteration on improving the weights to get a satisfactory controller, using the process detailed in Section 2.2. Two controllers were designed, for the operating points at $0.5\mathcal{P}_n$ and $0.99\mathcal{P}_n$, that is G_{δ_1} is replaced by the design models $G_0 \simeq G|_{\delta_1=-1}$ and $G_2 \simeq G|_{\delta_1=.998}$, respectively. The minimization is carried out iteratively resulting in suboptimal $\mathcal{H}_\infty$ controllers achieving a closed-loop ∞-norm of approximately 17.6 and 16, respectively. To meet the robust performance objective given in Equation 14, the weights need

to be scaled by approximately $\frac{1}{18}$. The weights were slightly different to optimize the performance at the different operating conditions. The corresponding augmented plant will be termed "P50" and "P99", while the controllers will be denoted by "H50" and "H99" in the sequel.

5.4 Robustness Analysis

Both $\mathcal{H}_\infty$ designs for H50 and H99 are analyzed with respect to structured uncertainty using μ [7]. The upper and lower bounds for μ are calculated on the closed-loop response of $P50 \star H50$ and $P99 \star H99$ using the following structure:

$$\mathbf{\Delta} = \left\{ \mathbf{diag}[\Delta_2, \quad , \Delta_3] : \Delta_2 \in \mathbb{C}^{2\times 2}, \Delta_3 \in \mathbb{C}^{5\times 6} \right\}$$

where Δ_2 and Δ_3 are the uncertainty and performance blocks, respectively. Recall the weights have been scaled as suggested in Section 5.3.

The upper and lower bounds for μ using $P50 \star H50$ with respect to this block structure are plotted in Figure 16 in solid lines (they lie on top of one another). Furthermore, the maximum singular values for robust stability (dashed) and nominal performance (mixed) as defined in Equations (11) and (13) are shown in the same plot. Similar bounds are obtained using $P99 \star H99$. Since they are close to those shown in Figure 16, they are not included in this paper.

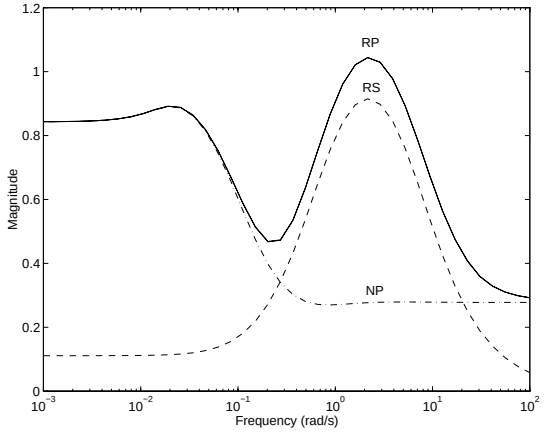

Figure 16: μ bounds for robust performance (RP) and maximum singular values for robust stability (RS) - nominal performance (NP). The bounds for μ are plotted in solid lines, and the maximum singular values for RS and NP are shown in dashed and mixed lines, respectively.

6 LPV Synthesis

Once the parameterized model G_{δ_1} is obtained, the controller design becomes similar to the $\mathcal{H}_\infty$ design of the previous section. The synthesis structure used is the same as for the $\mathcal{H}_\infty$ synthesis, shown in Figure 14, with uncertainty and performance weights included (see Figure 15). The

values these weights take for the LPV design are

$$W_m = \frac{800\mathbf{s}+20}{\mathbf{s}+10} I_2^1 \quad W_p = \mathbf{diag}\left[\frac{0.01(\mathbf{s}^2+1.2522\mathbf{s}+0.8)}{\mathbf{s}^2+0.0056\mathbf{s}+1.610^{-5}}, 8, AO(\delta), 0.5I_2\right]^1$$

Placing the augmented plant model in the form of Equation 3 results in a system shown in Figure 4, where $n_0 = 7$ and $n_1 = 6$, that is $\Delta = \mathbf{diag}[\mathbf{z}^{-1}I_7, \quad \delta_1 I_6]$.

In general, for a system with widely varying dynamics, the same performance requirements over the entire operating range may not be desirable or provide adequate performance. For LPV synthesis, the solution to this problem is to incorporate parameter variations (depending on δ_1) into the weights. This may be inadvisable, however, because including a δ-dependence in the weight increases the size of the time-varying perturbation block, which may degrade performance. Thus the applicability of this technique must be determined on a problem-by-problem basis.

For the PWR, the same performance requirements over the entire operating range are not desirable. At low power, the axial offset can be minimized much better than at high, as previously noted. Thus the weight on the axial offset will contain a weight depending on δ_1, which requires higher performance at low power than at high power. This weight is shown, as a function of δ_1, in Figure 17.

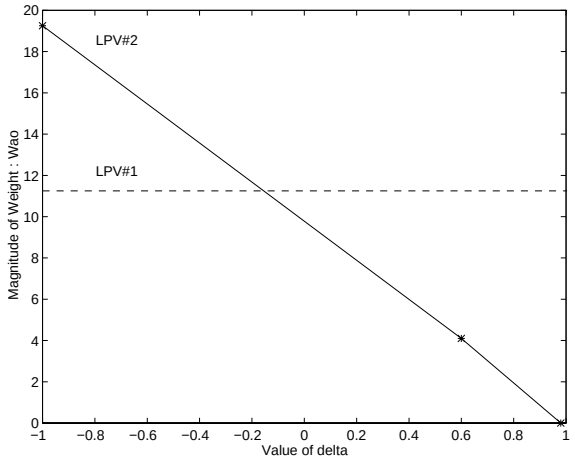

Figure 17: Performance weight on the axial offset as a function of δ_1, where $\mathcal{P} = (\delta_1 + 3)/4$. A '*' shows a value corresponding to $0.5\mathcal{P}_n$, $0.9\mathcal{P}_n$, or $0.99\mathcal{P}_n$.

Two controllers were designed. The first is called "LPV #1" and is an LPV controller with the constant weight on the axial offset as shown in Figure 17 in dashed line. The second is called "LPV #2" and uses the same weights as LPV #1, except W_{AO} was allowed to depend on the operating power, according to Figure 17 in solid line.

For a given open-loop interconnection, we can compare the LTI $\mathcal{H}_\infty$ performance level for the various designs. We consider the open-loop interconnection used for LPV #2 and close the loop with each controller. The values obtained over the whole operating range are shown in Figure 18. For each linear time-invariant design, the best performance level is obtained in the power range

corresponding to the nominal model used for the synthesis, that is H50 does better at low power while H99 does better at high power. The graph on the left side in the same Figure, gives a closer look at the LPV designs (the LTI designs are omitted). Note that LPV #2 achieves a better performance level at low power. This reflects the original intent for adding a delta in the performance weight.

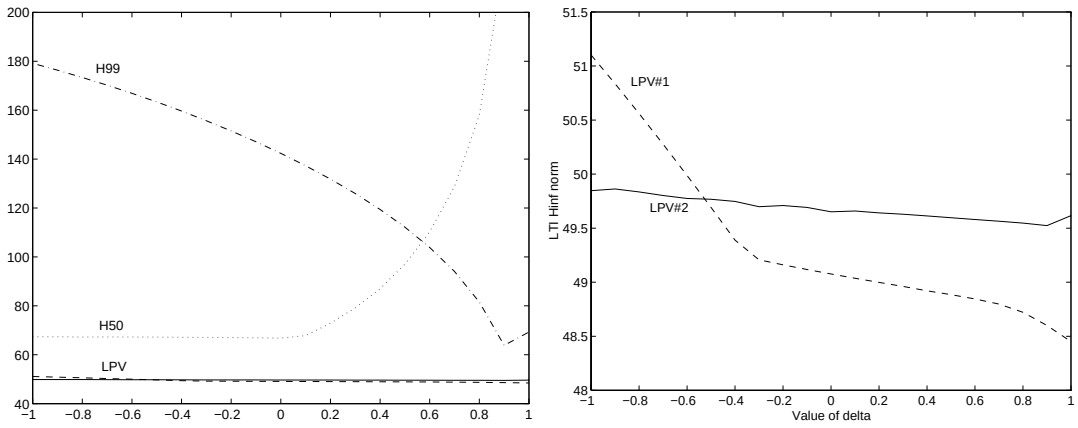

Figure 18: LTI $\mathcal{H}_\infty$ performance level of controllers on LFT model: $\mathcal{H}_\infty$ controllers, H50 (dotted) and H99 (mixed), and LPV#1 (dashed) and LPV#2 (solid).

7 Evaluation

In this section we evaluate the LPV controllers by comparing them with the $\mathcal{H}_\infty$ controllers, H50 and H99.

Figure 19 shows the step responses of the closed-loop systems consisting of each of the controllers and a linearization of the plant at $0.99\mathcal{P}_n$. Note that both LPV controllers are locked at $\delta_1 = .998$. Step responses are shown because we are interested in the low frequency rejection properties of the closed-loop system. The magnitude of the step is chosen to facilitate the comparison with NL simulations in the sequel. In the first column of plots, the dotted lines are the reference signals, the dashed lines are the responses with the first LPV controller, the solid lines are with the second LPV controller, and the mixed lines are with H99. The second column of plots shows u_1 and u_2 for each of the controllers; u_1 is the solid line and u_2 the dashed one. Figure 20 is identical to Figure 19 except that the responses are with respect to a linearization of the plant at $0.5\mathcal{P}_n$ and both LPV controllers are locked at $\delta_1 = -1$.

At high power the plant is more difficult to control, because the control rods are almost withdrawn from the reactor. Referring to Figure 19, the LPV controllers are almost identical in behavior. They perform equally well, but are not as fast as H99, although they have no overshoot on the temperature. The noticeable difference is that the LPV controllers have less axial offset than H99. At this power, we consider LPV #2 the best of these controllers.

Some of this behavior is preserved in Figure 20, but the model is quite different here. Here H50 is slightly faster than the LPV controllers. The major difference at this power is that u_2 now has more control authority than u_1, so controllers do better to use it more, since this results in lower axial offset. H50 does use u_2 more, and the axial offset is considerably lower. At this operating point, we consider H50 the best controller.

At low power, u_2 is the dominant control, but as the power increases u_1 should be used more and more to better meet the control objectives. The LPV controllers do not change strategy between these operating points. Notice that the control plots for LPV #2 are almost identical, up to a scale change in magnitude. This is a result of the worst-case nature of LPV controllers. Even though, LPV controllers are indeed parameter-dependent, the change in the gain of the controllers when the parameter varies from high power too low power is too restricted. Since achieving worst-case performance does not require a change of strategy, and may in fact forbid one, the controllers do not change their use of the inputs. An attempt to alleviate this problem is to use synthesis techniques that incorporate *a priori* bounds on the parameter rate of variation [23]. Preliminary results lead to less conservative designs [24].

Next, the behavior of the LPV controllers on a nonlinear simulator of the PWR is shown. Also, control systems for a PWR normally have dead-bands included to prevent moving the control rods for small changes in operating conditions. These, as well as saturations on the controls, would require the use of specific conditioning techniques to guarantee anti-wind up bumpless transfer. These aspects lie beyond the scope of this paper and complementary investigations are underway. Hence, saturations and dead-bands have been removed, for the purposes of this study. Finally, the control system contains a static nonlinearity on u_2 which reflects an *a priori* knowledge on its loss of effectiveness as the power increases. The nonlinearity proved necessary in the identification of the models, and the control system simply inverts it out. In particular, this will explain the larger magnitude of u_2 at high power (the nonlinearity is unity at low power).

Figures 21 through 23 show the NL simulation results. In these figures, the response of LPV#1 is shown in dashed lines, the response of LPV#2 is shown in solid lines, and the references are shown in dotted lines. Also, u_1 is shown in solid lines, and u_2 in dashed lines. Figure 21 shows the response to a one percent step down around $0.99\mathcal{P}_n$. LPV#2 is faster, and introduces slightly less axial offset. This difference is even more noticeable in Figure 22, which is a five percent step at $0.5\mathcal{P}_n$. Comparing these results to the LTI simulations, we see that there is overshoot and the response is slower. LPV#2 clearly outperforms LPV#1 in the NL simulations.

Finally, the response of the LPV controllers to a large transient is shown in Figure 23. This is a ramp of -5%/minute from $\mathcal{P}_n$ to $0.5\mathcal{P}_n$. For comparison, we performed an *ad hoc* controller design (see [24]) that interpolates the gains of H50 and H99, based on $b_{v2}(\delta)$ in Figure 13. This *ad hoc* controller is noted "H50H99" in the sequel and is given by $H50H99 = \alpha(\delta)H50 + (1 - \alpha(\delta))\,H99$ where $\alpha(\delta) = \frac{b_{v2}(\delta) - b_{v2}(-1)}{b_{v2}(1) - b_{v2}(-1)}$. The idea is to develop a control law which smoothly schedules

between the output of these two controllers, using some interpolation scheme, based on the current power level. There is not much difference in either LPV controller on this trajectory. This is not surprising as stability for large transients is inherent in the LPV methodology, provided that the synthesis model is accurate over the operating range. The *ad hoc* controller has much less effect on the axial offset since it uses more v_2 and much less v_1. However, it does not track the reference on the temperature as well, thus facilitating the minimization on the axial offset.

A final validation on an actual plant would definitely be considered if allowable. As a matter of fact, safety regulations prevent us from testing new advanced controllers, especially those with an impact on the primary circuit. Therefore, real experimental data cannot be included and realistic simulators are used instead.

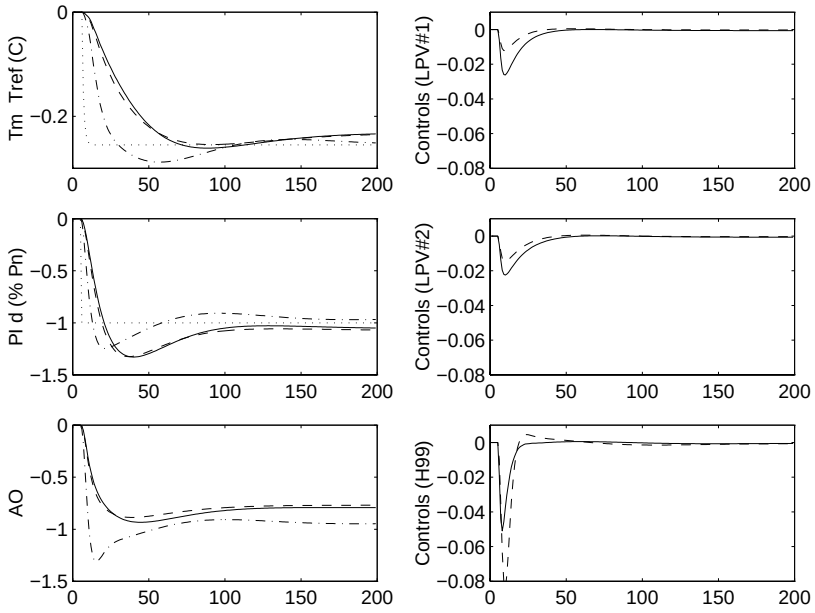

Figure 19: Comparison of Three Controllers at $0.99\mathcal{P}_n$. LPV#1 (dashed) - LPV#2 (solid) - H99 (mixed)

8 Concluding remarks

A preliminary objective for this study was to assess the effectiveness of an $\mathcal{H}_\infty$ controller based on a low-order model to control a pressurized water reactor. Of particular importance, the physical system was identified from NL simulation data using a MIMO identification-oriented state-space realization. The resulting model has been reduced using a frequency-weighted balanced realization technique.

A fixed LTI controller cannot maintain performance over the entire operating range. Hence, we have constructed an LPV controller which performs well, although not ideally, over the plant's operating range. This involved the construction of a parameter-dependent model from identified

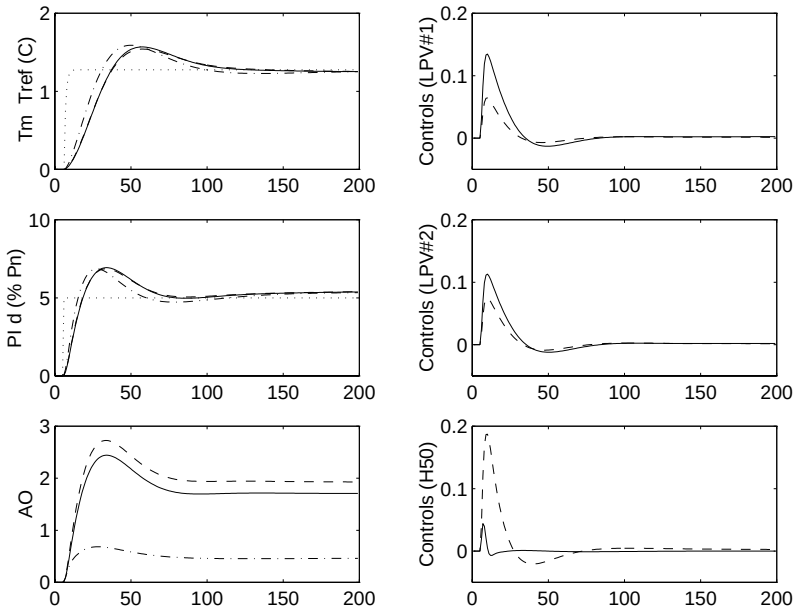

Figure 20: Comparison of Three Controllers at $0.5\mathfrak{P}_n$.LPV#1 (dashed) - LPV#2 (solid) - H50 (mixed)

models, and the development of a parameter-dependent weight on its performance. The LPV controller is able to do better over the entire operating range of the power plant than a single LTI design, but does not switch strategies in its use of the control rods from low to high power, a behavior we would prefer. This is attributable to the worst-case nature of the designs. Using an *ad hoc* gain-scheduled controller, that intrinsically changes strategies, leads to less conservative results in practice. However, such design provides no *a priori* guarantee of stability with respect to the rate of variation of the parameter. In fact, less conservative designs could be obtained using synthesis techniques that incorporate *a priori* bounds on the parameter rate of variation [23] as shown in [24].

References

[1] P. Bendotti and C. Beck, "Modelling and control of a pressurized water reactor using μ-synthesis," in *Proc. IFAC*, (San Francisco, CA), pp. O:103–108, 1996.

[2] P. Bendotti and E. Irving, "Modélisation simplifiée et commande du circuit primaire des REP," Tech. Rep. HI/20/93/008, Electricité de France, Aug. 1993.

[3] P. Bendotti and B. Bodenheimer, "Identification and $\mathcal{H}_\infty$ control design for a pressurized water reactor," in *Proc. IEEE CDC*, (Orlando, FL), pp. 1072–1077, 1994.

[4] R. E. Bodenheimer, Jr., *The Whirling Blade and the Steaming Cauldron.* PhD thesis, California Institute of Technology, June 1995.

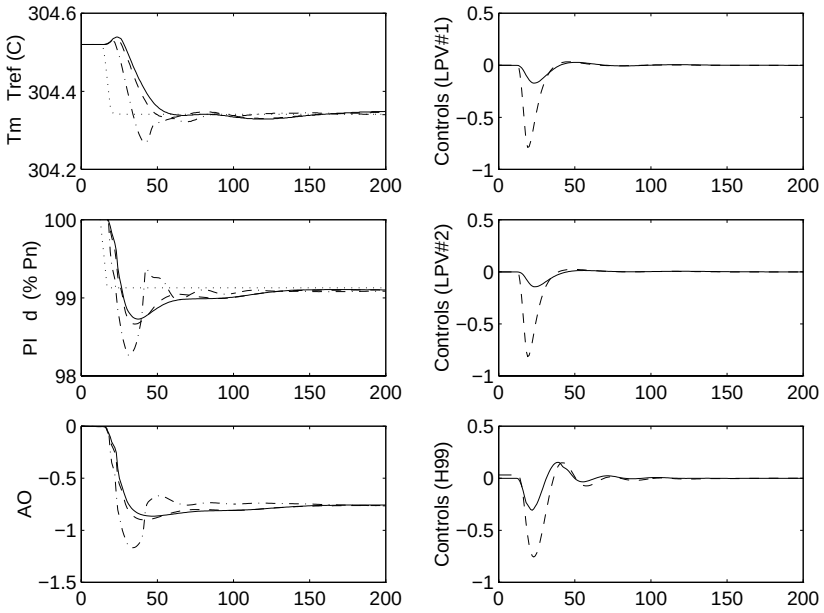

Figure 21: Comparison of Three controllers on a NL simulation to a step around $0.99\mathfrak{P}_n$.LPV#1 (dashed) - LPV#2 (solid) - H99 (mixed)

[5] B. Bodenheimer and P. Bendotti, "Optimal linear parameter-varying control design for a pressurized water reactor," in *Proc. IEEE CDC*, (New Orleans, LA), pp. 1072–1077, 1995.

[6] J. C. Willems, *The Analysis of Feedback Systems*. Cambridge, Massachusetts: M.I.T. Press, 1971.

[7] A. Packard and J. C. Doyle, "The Complex Structured Singular Value," *Automatica*, vol. 29, pp. 71–109, Jan. 1993.

[8] J. Doyle, K. Glover, P. Khargonekar, and B. Francis, "State-space solutions to standard $\mathcal{H}_2$ and $\mathcal{H}_\infty$ control problems," *IEEE Trans. Aut. Control*, vol. 34, pp. 831–847, Aug. 1989.

[9] A. Packard, "Gain-scheduling via linear fractional transformations," *Systems and Control Letters*, vol. 22, pp. 79–92, 1994.

[10] R. Redheffer, "On a certain linear fractional transformation," *Journal of Mathematical Physics*, vol. 39, pp. 269–286, 1960.

[11] M. G. Safonov, "Stability margins of diagonally perturbed multivariable feedback systems," *IEE Proceedings*, vol. 129-D, no. 6, pp. 251–155, 1982.

[12] J. C. Doyle, "Analysis of feedback systems with structured uncertainties," *IEE Proceedings*, vol. 129, Part D, no. 6, pp. 242–250, 1982.

[13] K. Zhou, J. Doyle, and K. Glover, *Robust and Optimal Control*. N. J.: Prentice-Hall, 1995.

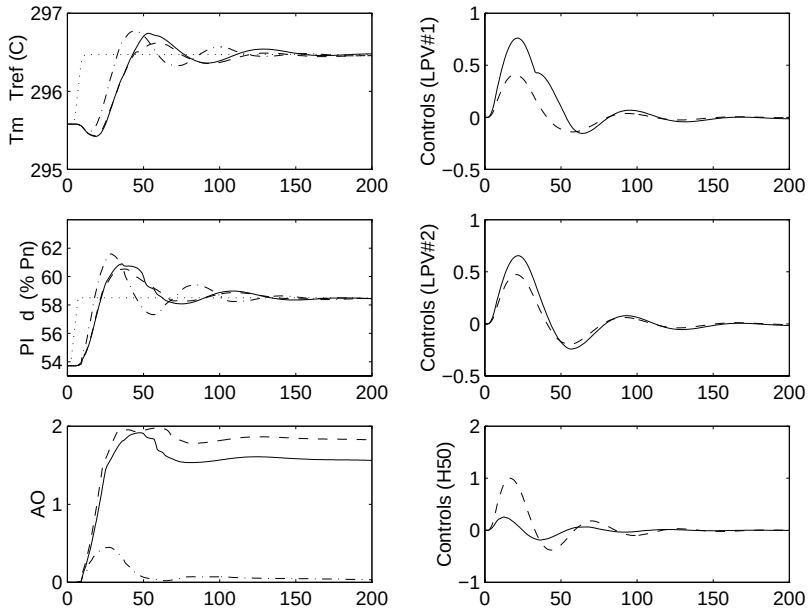

Figure 22: Comparison of LPV controllers on a NL simulation to a step around $0.5\mathfrak{P}_n$. LPV#1 (dashed) - LPV#2 (solid) - H50 (mixed)

[14] S. Boyd, L. E. Ghaoui, E. Feron, and V. Balakrishnan, *Linear Matrix Inequalities in System and Control Theory*. Philadelphia: SIAM, 1994.

[15] F. Paganini and J. Doyle, "Analysis of implicit uncertain systems," in *Proc. IEEE CDC*, (Orlando, FL), pp. 3673–3678, 1994.

[16] W. Lu, *Control of Uncertain Systems: State-Space Characterizations*. PhD thesis, California Institute of Technology, 1995.

[17] W. Lu, K. Zhou, and J. Doyle, "Stabilization of linear uncertain systems: An LFT approach," *IEEE Trans. Aut. Control*, 1996.

[18] K. Glover and J. C. Doyle, "A state space approach to $\mathcal{H}_\infty$ optimal control," in *Three Decades of Mathematical Systems Theory: A Collection of Surveys at the Occasion of the 50th Birthday of J. C. Willems* (H. Nijmeijer and J. M. Schumacher, eds.), vol. 135 of *Lecture Notes in Control and Information Sciences*, New York: Springer-Verlag, 1989.

[19] P. Bendotti and C. Beck, "LFT Model reduction and Controller Synthesis for a Pressurized Water Reactor," in *Proc. IEEE CDC*, (Kobe, Japan), 1996.

[20] L. Ljung, *System Identification, Theory for the User*. Englewood Cliffs, New Jersey: Prentice Hall, 1987.

[21] B. Moore, "Principal component analysis in linear systems: Controllability, observability, and model reduction," *IEEE Trans. Aut. Control*, vol. 26, no. 1, pp. 17–31, 1981.

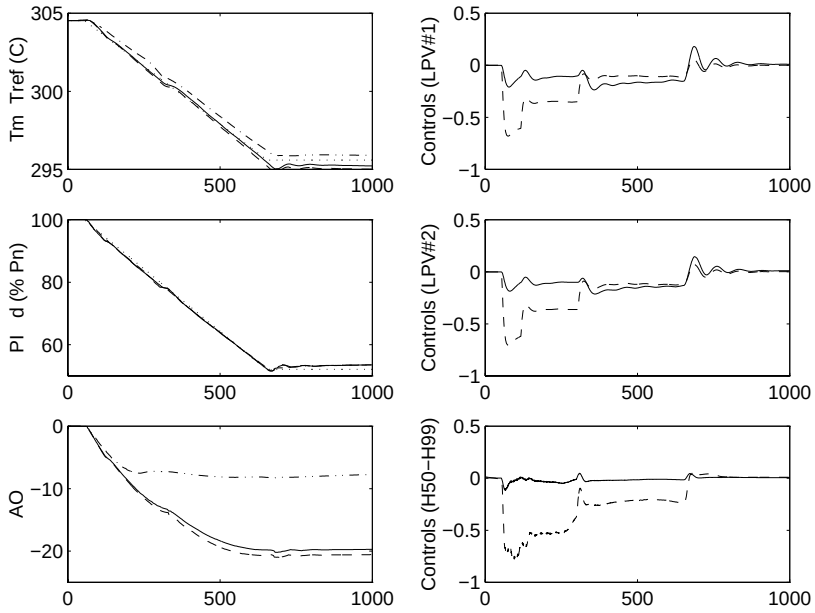

Figure 23: Comparison of LPV controllers on a NL simulation to a large transient. LPV#1 (dashed) - LPV#2 (solid) - H50H99 (mixed)

[22] D. F. Enns, "Model reduction with balanced realizations: an error bound and a frequency weighted generalization," in *Proc. IEEE CDC*, vol. 2, pp. 127–132, 1984.

[23] F. X. Wu, A. Yang, A. Packard, and G. Becker, "Induced $\mathcal{L}_2$ norm control for LPV systems with bounded on parameter variation rates," in *Proc. ACC*, 1995.

[24] G. Becker, P. Bendotti, P. Gahinet, and C.-M. Falinower, "Analysis and controller synthesis for a pressurized water reactor using linear parameter varying systems," in *Proc. IEEE CDC*, (Kobe, Japan), 1996.